GIS-Based Analysis of the Potential Effectiveness and Efficiency of Mobile Terrestrial LiDAR to Survey and Monitor Rockfall Areas Along 15 km of Highway E45

Edgar Ferro[1], Francesco Cemin[1], Leonardo De Rosa[2], Alessandro Corsini[2], Francesco Ronchetti[2], Francesco Lelli[2], Alfonso Vitti[1], and Lucia Simeoni[1](✉)

[1] Department of Civil, Environmental and Mechanical Engineering, University of Trento, Trento, Italy
lucia.simeoni@unitn.it

[2] Department of Chemical and Geological Sciences, University of Modena and Reggio Emilia, Modena, Italy

Abstract. A method was developed in a GIS environment to assess the potential effectiveness and efficiency of a mobile terrestrial LiDAR survey at detecting the geometrical changes due to rockfalls from the cliffs facing a 15 km stretch of a highway in an alpine valley. The elements exposed to rockfalls were automatically classified as viaduct or open-sky ground supported road by comparing the DTM with the DSM. The most critical cliffs were then identified through the analysis of the rockfall trajectories. For these cliffs two mobile terrestrial LiDAR surveys from a vehicle travelling on the highway were simulated: a stop&go survey and a kinematic survey. The effectiveness of the surveys was assessed in terms of sensed area and density of the measured points. Their efficiency was specified in terms of feed rate. For both surveys at least 70% of the cliffs was visible with a point density higher than 400 points/m^2. The proportion of sensed area and density of the points provided by the stop&go survey was slightly higher compared with the kinematic survey, but the feed rate for the kinematic survey was higher.

Keywords: Rockfall · highway · mobile terrestrial LiDAR · effectiveness · efficiency

1 Introduction

The European Route E45 runs through the Brenner Pass in the Alps and enters Italy through the Isarco Valley, taking the national designation A22. Here, the A22 highway runs often on viaducts and through tunnels. The Isarco Valley has the typical U-shaped profile of glacial valleys and cliffs that, locally, are steeper than 70°. This usually occurs where the valley crosses the Permian ignimbrite and tuff.

Rockfalls are major natural hazards in this valley [1] and may interact with the highway, causing disruption and posing harm to its users. Periodical surveys of the rock

A. Ferrari et al. (Eds.): CNRIG 2023, SSGG, pp. 194–201, 2023.
https://doi.org/10.1007/978-3-031-34761-0_24

cliffs can potentially identify the areas susceptible to rock detachment and allow to estimate the volume of the unstable blocks. This information could be used as an input for risk assessment and protection work design [2]. This study investigates the potential of mobile terrestrial Light Detection And Ranging (LiDAR) from a vehicle moving along a 15-km long stretch of the A22 highway to survey periodically the rock cliffs, identify those most susceptible to rockfalls that may interact with the highway and hence provide the infrastructure manager with a tool that informs risk mitigation strategies. A rockfall-highway interference analysis was carried out to identify the elements of the highway infrastructure exposed to rockfalls. Then numerical simulations in a Geographic Information System (GIS) environment were performed to assess the potential effectiveness and efficiency of stop&go and kinematic LiDAR surveys. Other techniques, such as LiDAR surveys from an Unmanned Aerial Vehicle (UAV) or helicopter, were not considered due to the flight restrictions above the highway and the unfavourable morphology of the Isarco Valley with very steep cliffs.

2 Rockfall-Highway Interferences

2.1 Classification of Elements Exposed to Rockfalls

The open-source GIS software QGIS was used to identify the three main types of highway infrastructure: (1) tunnel, (2) viaduct and (3) open-sky, ground-supported road.

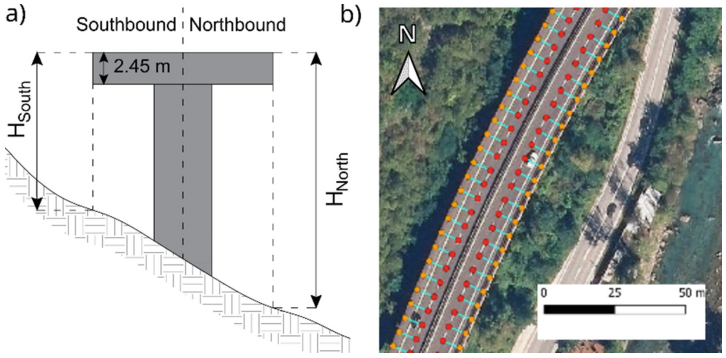

Fig. 1. Height H to recognize viaducts and ground supported roadways. a) Sketch showing the heights for southbound and northbound as the difference between roadway and ground elevations, b) couples of points used to calculate the heights: orange point = ground point from DTM, red point = roadway point from DSM.

The tunnels were indicated in a shapefile freely available from [1] and their position was verified by comparison with orthophotos. The viaducts and stretches of open-sky ground-supported road were distinguished based on the value of H, the minimum between H_{South} and H_{North} shown in Fig. 1a. These were calculated as the difference between the elevations of a roadway point and a ground point, i.e. the coupled red and orange points, respectively, shown in Fig. 1b. The road point elevation was taken from

the Digital Surface Model (DSM) and the ground point elevation from the Digital Terrain Model (DTM), both with spatial resolution of 0.5 m and freely downloaded from [1]. Values of H greater than 2.5 m (slightly higher than the height of the decks of the viaducts) were associated with viaducts, lower values with open-sky, ground-supported road. For the viaducts, the positions of the piers were also represented in QGIS.

It was found that, of the 15 km length of the A22 highway between the 58-km and 72-km markers, 55% runs on viaducts, 13% in tunnels and 32% consists of open-sky, ground-supported road.

2.2 Potential Impact of Rockfalls Against Exposed Elements

The expected trajectories of single-block rockfalls that can potentially detach from subvertical rock cliffs were simulated using RocPro3D software [3]. Cliffs sloping more than 70° were identified as the most susceptible to rockfalls, then simulations were carried out for a total of 55 different potential source zones using as input data: a DTM at 2.5 m resolution [1]; a map of the potential source zones; a map of soil types with associated reference normal and tangential restitution coefficients estimated on the basis of values proposed by [4]; a map of rockfall barriers and protections (with location, height and impact resistance from the VISO inventory [5]). Rockfall simulations were carried out for blocks with reference diameters of 0.5 m and 2.0 m, and allowed to map and assess trajectories, bounce heights and impact energies with respect to these two block dimension scenarios. The simulations adopted a uniform probabilistic approach, i.e. variation of normal and tangential restitution coefficients and other soil physical parameters such as dynamic friction, lateral deviation and rebounds flattening on the basis of the velocity of the rockfall, which considers that each parameter value has the same occurrence probability within its variation range, hence: $\varepsilon_p = \varepsilon + \Delta\varepsilon \cdot U(-1, +1)$, where $\Delta\varepsilon$ is the parameter variation and $U(-1, +1)$ is the uniform distribution between -1 and $+1$ sampled from a random number generator (with a seed of about $1.84e^{19}$). The parameter variation $\Delta\varepsilon$ is in turn dependent on the incident velocity following a model, which allows taking into account a larger uncertainty at low velocities compared to high velocities.

Depending on the extension of potential rockfall source areas, a different number of possible detachment points and associated trajectories were simulated ($<$4000 m^2: 1000 trajectories; 4000–13000 m^2: 1500 trajectories; 13000–20000 m^2: 2000 trajectories; $>$20000 m^2: 2500 trajectories). The simulation results for blocks with 0.5 m and 2.0 m reference diameters were exported to GIS, as 2.5-m resolution raster maps of rockfall trajectories, energies and bounce heights.

To assess the possible interaction between the rockfalls and the highway, the positions of the viaduct piers were rasterized at 2.5 m spatial resolution. Also, the height of the roadway with respect to the ground was calculated by subtracting the DSM elevation from the DTM elevation.

By GIS-based spatial intersection between the maps of rockfall energy and the map of the pier positions, maps of the points (i.e. cells) where rock blocks can collide with the piers with a given energy were obtained for the 0.5 m and 2 m diameter scenarios. Moreover, the intersection between the maps of rockfall bounce height and the map of

the roadway elevation, allowed to identify the points where rockfalls blocks can bounce over and onto the road pavement.

In the 15-km stretch of the highway, 10 cliffs were recognized as sources of the most dangerous rockfalls. Examples of simulation results are shown in Fig. 2. Overall, the simulations showed that the interaction between rockfalls and viaduct piers is possible at several locations along the 15-km stretch of the A22 highway considered in this study. Less likely are the rock blocks bouncing onto the road. These results are obtained by assuming, in the simulations, that the existing rockfall barriers are capable of stopping the intercepted rock blocks whose kinematic energy is lower than the nominal energy that can be absorbed by the barriers.

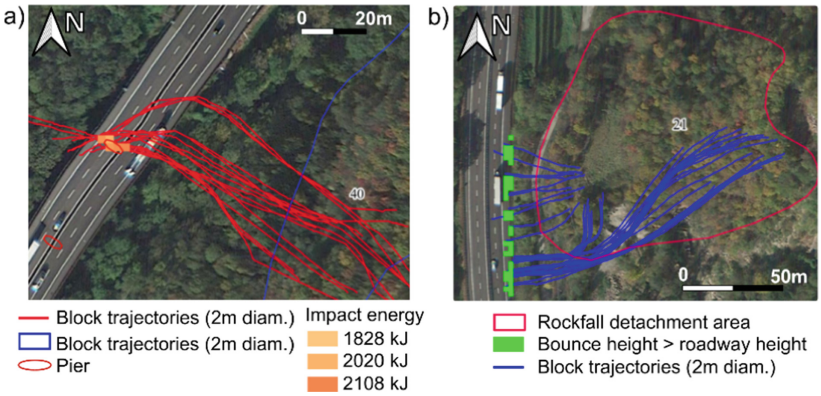

Fig. 2. Rockfall-highway interference for the 2-m block diameter scenario: a) impact between the rock blocks and the piers; b) rock blocks bouncing onto the roadway.

3 Simulations of Mobile Terrestrial LiDAR Surveys

Using GIS software tools, two different types of LiDAR survey from a vehicle moving on the breakdown lane (the outer lane) of the A22 highway were simulated: (1) a stop&go survey [6, 7] and (2) a kinematic survey [8] at 15 km/h. The surveys were simulated for the 10 cliffs recognised as the source of the most critical rockfall-infrastructure interferences. Below, the algorithm used in the simulations is briefly described, while greater detail can be found in [9].

The simulations were performed in GRASS GIS environment [10] with the support of Python scripts. The DEM used in the analyses was created by combining the DTM and the DSM provided by [1]: the elevations from the DSM were assigned to the cells located on the roadway, while the DTM elevations were assigned to the remaining cells. The DSM and DTM used as input and the output DEM had spatial resolution (cell size) of 0.5 m. For each cliff, points corresponding to the positions of the vehicle equipped with the laser scanner were created along the breakdown lanes with a pitch L = 1 m for the kinematic survey and L = 20 m for the stop&go survey; the height h of the laser scanner (the *observer point*) from the pavement was assumed equal to 1.75 m (Fig. 3a).

The GRASS GIS command *r.viewshed* was used to calculate the angle φ between the direction of the horizontal at the *observer point* and the direction of the segment joining the *observer point* to a cell on the cliff (the *observed point*) for each cell of the DEM visible from the *observer point* (Fig. 3b). A lower bound value of $-5°$ was assumed for φ to account for the guardrail, road pavement and other obstructions.

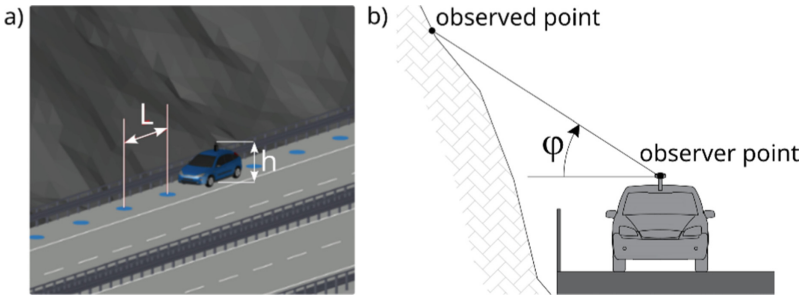

Fig. 3. Mobile terrestrial LiDAR from the breakdown lane: a) vehicle positions (blue points on the breakdown lane) with pitch L equal to 1 m for the kinematic survey and 20 m for the stop&go survey; b) angle φ used to detect the visible cells of the DEM.

A RIEGL VZ-2000i was used for the simulations of the stop&go survey, a RIEGL VUX-1HA for the kinematic survey. Their instrumental variables - minimum and maximum LiDAR distances ($d_{\min}$ and $d_{\max}$), vertical field of view from the the horizontal (FOV), sample frequency (nr_{pps}) and scanning speed (nr_{rps}) - are listed in Table 1.

Table 1. Technical specifications of the laser scanners RIEGL used for the simulations.

Instrument variable	RIEGL VZ-2000i (stop&go survey)	RIEGL VUX-1HA (kinematic survey)
Min-Max distances $d_{\min} - d_{\max}$ [m]	1–600	1–235
Vertical field of view FOV [°]	100 (+60, −40)	360°
Sample frequency nr_{pps} [pts/s]	Up to 500.000	Up to 1.800.000
Scanning speed nr_{rps} [rps]	Up to 240	Up to 250

The distance *dp* along a scan line between points located at a distance *d* from the laser scanner can be calculated as:

$$dp = \frac{nr_{rps}}{nr_{pps}} \cdot \text{FOV} \cdot d \tag{1}$$

where the FOV is expressed in radians.

For the stop&go survey with the RIEGL VZ-2000i, all the cells within the field of view (φ between $+60°$ and $-40°$) and with *d* between $d_{\min}$ and $d_{\max}$ (i.e. in the range 1–600 m) were assumed visible. The angle β and the distance *ds* between the scan lines

were calculated assuming the instrument to perform a 360° (2π) horizontal rotation in 60 s:

$$\beta = \frac{2\pi/60\,\mathrm{s}}{nr_{rps}} \tag{2}$$

$$ds = d \cdot sen\beta \tag{3}$$

For the kinematic survey with the RIEGL VUX-1HA, all the cells with a distance d from the scanner between $d_{\min}$ and $d_{\max}$ (i.e. in the range 1–235 m) and an angle $\varphi > -5°$ were considered visible. The distance between the scan lines ds was calculated as:

$$ds = v/nr_{rps} \tag{4}$$

with $v = 15$ km/h (4.17 m/s).

Finally, for both the kinematic and stop&go surveys the density of the points that can be potentially sensed per m^2 ($nr_{points\_m^2}$) was calculated as:

$$nr_{points\_m^2} = \frac{1}{ds \cdot dp} \cdot cos\psi \tag{5}$$

where ds and dp are expressed in meters and ψ is the angle between the vector V_1, parallel to the segment joining the *observer point* and the *observed point*, and the vector V_2, perpendicular to the *observed point*.

4 Results

4.1 Effectiveness

Considering all the 10 investigated cliffs, the stop&go survey was able to sense more than 90% of the surface area sloping more than 70°. For more than 90% of this area, the point density resulted higher than 400 points/m^2. For the cliff close to the 70-km marker, the area sensed by the stop&go survey is shown in Fig. 4a and Fig. 4b, where the sensed cells of the DEM are shown in blue (a darker blue indicates a higher point density). Figure 4a shows the point density for the whole visible area of the cliff, Fig. 4b only for the parts of the cliff sloping more than 70°.

The kinematic surveys detected more than 85% of the area sloping more than 70°, with more than 70% of this area characterised by a point density larger than 400 points/m^2 and almost all of it with a point density larger than 100 points/m^2. For the cliff near the 70-km marker, the area sensed by a kinematic survey is shown in red in Fig. 4c and Fig. 4d, where darker red corresponds to higher point densities. Figure 4c shows the overall sensed area, Fig. 4d only the parts of the cliff sloping more than 70°.

4.2 Efficiency

The two LiDAR instruments considered in the simulations can achieve similar performances in terms of 3D position accuracy and precision. For the kinematic survey

positioning is mainly constrained by GPS/IMU performance which, however, should be adequate for the specific purpose of this study. Key differences between the two survey methods are:

- the scan speed, higher for the kinematic survey;
- the feed rate, higher for the kinematic survey;
- the maximum distance and accuracy/precision, higher for the stop&go survey;
- the point density, higher for the stop&go survey.

Owing to the higher feed rate, the kinematic survey is expected to reduce the time required to execute the survey and hence, the man hours and the occupation time of the breakdown lane. Moreover, the safety measures are simpler for the kinematic survey, in which the vehicle equipped with the laser scanner does not need to stop and the surveyors are not required to leave the vehicle, exposing themselves to a greater danger. Although the kinematic survey is characterized by a smaller distance of the *observed points* and a lower accuracy/precision, it remains suitable for monitoring rock cliffs susceptible to rockfalls that might endanger the highway. Overall, the kinematic survey seems more efficient.

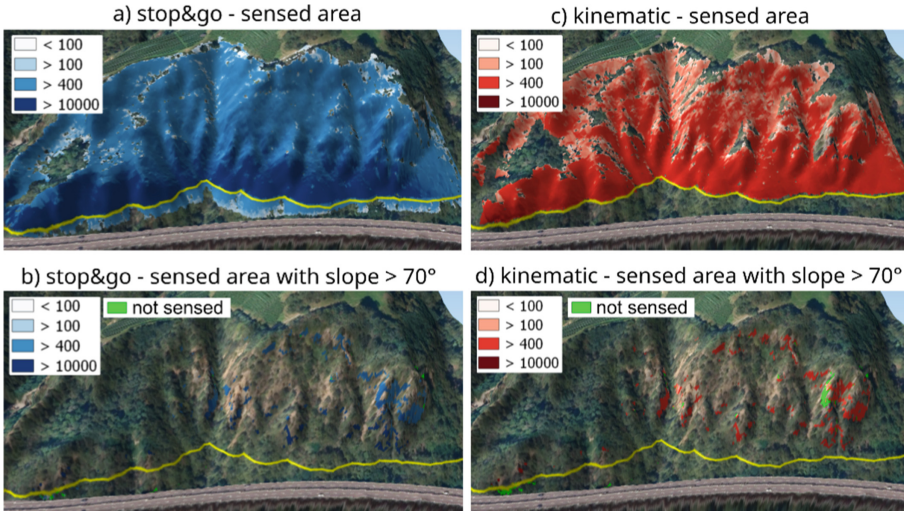

Fig. 4. Simulated LiDAR surveys of the cliff at the 70-km marker; a) cliff area sensed by stop&go survey; b) cliff area sloping more than 70° sensed by stop&go survey; c) cliff area sensed by kinematic survey; d) cliff area sloping more than 70° sensed by kinematic survey; different point density (points/cell) are indicated with different color intensity, as indicated in the legend.

5 Conclusion

Numerical simulations in a GIS environment have shown that mobile terrestrial LiDAR from a vehicle moving slowly along a breakdown lane can be potentially used to survey periodically the rock cliffs susceptible to rockfalls that may be present close to a highway.

A stop&go survey was found able to sense over 90% of the cliff areas sloping more than 70°, 90% of which with a point density greater than 400 points/m^2. A similar performance was achieved with a kinematic survey, which could sense over 85% of the cliff area sloping more than 70%, 70% of which with a point density larger than 400 points/m^2 and almost all of it with a point density larger than 100 points/m^2. Despite the smaller point density, the kinematic survey seems the most convenient, as it can be carried out more quickly and with simpler safety measures. Moreover, for the kinematic survey the point density could be increased by performing multiple scans of the most critical cliffs.

Funding. This research was funded by Autostrada del Brennero S.p.A (Brenner Autobahn AG) and partly by MUR PON R&I 2014–2020 Program (project MITIGO, ARS01_00964).

References

1. Rete Civica Alto Adige. http://geoportale.retecivica.bz.it. Accessed 13 Dec 2022
2. Macciotta, R., Martin, C.D., Morgenstern, N.R., Cruden, D.M.: Quantitative risk assessment of slope hazards along a section of railway in the Canadian Cordillera—a methodology considering the uncertainty in the results. Landslides **13**(1), 115–127 (2015). https://doi.org/10.1007/s10346-014-0551-4
3. RocPro3D. http://www.rocpro3d.com. Accessed 29 May 2023
4. Crosta, G.B., Agliardi, F.: A methodology for physically based rockfall hazard assessment. Nat. Hazard. **3**, 407–422 (2003). https://doi.org/10.5194/nhess-3-407-2003
5. VISO. https://maps.civis.bz.it/?context=PROV-BZ-HAZARD. Accessed 13 Dec 2022
6. Abellán, A., Calvet, J., Vilaplana, J.M., Blanchard, J.: Detection and spatial prediction of rockfalls by means of terrestrial laser scanner monitoring. Geomorphology **119**, 162–171 (2010). https://doi.org/10.1016/j.geomorph.2010.03.016
7. Kromer, R.A., Hutchinson, D.J., Lato, M.J., Gauthier, D., Edwards, T.: Identifying rock slope failure precursors using LiDAR for transportation corridor hazard management. Eng. Geol. **195**, 93–103 (2015). https://doi.org/10.1016/j.enggeo.2015.05.012
8. Lim, S., Thatcher, C.A., Brock, J.C., Kimbrow, D.R., Danielson, J.J., Reynolds, B.J.: Accuracy assessment of a mobile terrestrial lidar survey at Padre Island National Seashore. Int. J. Remote Sens. **34**(18), 6355–6366 (2013). https://doi.org/10.1080/01431161.2013.800658
9. Cemin, F.: Interazione pendio-autostrada a scala regionale: sviluppo di un sistema per la pianificazione di rilievi LiDAR e definizione delle condizioni al contorno idrauliche per lo studio di frane estremamente lente. Master's thesis, Department of Civil Environmental and Mechanical Engineering, University of Trento, Italy (2021)
10. GRASS Development Team. Geographic Resources Analysis Support System (GRASS) Software, Version 7.8. Open Source Geospatial Foundation (2020). https://grass.osgeo.org. Accessed 21 Feb 2023